Article

Not peer-reviewed version

# Evaluation of $Y_2O_3$:Eu@$SiO_2$ Nanoparticles as Photosensitizer for X-Ray Activated Photodynamic Therapy in Cancer

Hannah J. Zhang , Tristan Ide , Maharajan Sivasubramanian , Lara Leoni , Jeffrey S. Souris , Divya Brahmbhatt , Eve Tanios , Ariel Pan , Shih-Hsun Cheng , Nai-Tzu Chen , Leu-Wei Lo * , Chin-Tu Chen *

Posted Date: 24 May 2024

doi: 10.20944/preprints202405.1623.v1

Keywords: activated photodynamic therapy (PDT); X-ray activated PDT (XPDT); nanoparticle (NP); photosensitizer (PS); nano-PS; Europium doped Yttrium oxide nanoparticles ($Y_2O_3$:Eu); silica coated $Y_2O_3$:Eu ($Y_2O_3$:Eu@$SiO_2$); reactive oxygen species (ROS)

*Article*

# Evaluation of $Y_2O_3$:Eu@$SiO_2$ Nanoparticles as Photosensitizer for X-Ray Activated Photodynamic Therapy in Cancer

**Hannah J. Zhang [1,2], Tristan Ide [1], Maharajan Sivasubramanian [3], Lara Leoni [2], Jeffrey S. Souris [1,2], Divya Brahmbhatt [1,4], Eve Tanios [1], Ariel Pan [1,5], Shih-Hsun Cheng [1], Nai-Tzu Chen [1], Leu-Wei Lo [1,3,*] and Chin-Tu Chen [1,2,*]**

[1] Department of Radiology, The University of Chicago, Chicago, IL 60637, USA
[2] Integrated Small Animal Imaging Research Resource, Office of Shared Research Facilities, The University of Chicago, Chicago, IL 60637, USA
[3] Institute of Biomedical Engineering and Nanomedicine, National Health Research Institutes, Zhunan 35053, Taiwan
[4] Illinois Mathematics and Science Academy, Aurora, IL 60506
[5] Laboratory of Structural Biophysics and Mechanobiology, The Rockefeller University, New York, NY 10065, USA
* Correspondence: lwlo@nhri.org.tw (L.-W.L.); c-chen@uchicago.edu (C.-T.C)

**Abstract:** Traditional photodynamic therapy (PDT), a clinical cancer therapeutic approach using light in killing cancer cells, is often limited by insufficient light penetration, inefficient photosensitizer energy transfer, and inadequate oxygen in hypoxic tumors. Employing X-ray to activate photosensitizer in PDT can potentially overcome these limitations. Here, we compared protocols to synthesize a novel nano-photosensitizer composed of a europium-doped yttrium oxide core with a silica shell ($Y_2O_3$:Eu@$SiO_2$) which can be utilized in such therapeutic method, i.e., X-ray activated PDT (XPDT). Transmission electron microscopy (TEM) and dihydroethidium (DHE) were utilized to evaluate the effects of various synthesis conditions on the characteristics of $Y_2O_3$:Eu@$SiO_2$ and their ability to generate reactive oxygen species (ROS). The *in vivo* tumor suppression effects of the $Y_2O_3$:Eu@$SiO_2$ were assessed by $^{18}$F-fluorothymidine position emission tomography ($^{18}$F-FLT PET) in human ovarian cancer xenografts using radiation sensitive CAOV3 and radiation resistant SKOV3 cell lines. Our data revealed a positive correlation between nanoparticle condensation time and core size as well as a negative correlation between urea concentrations and core size. Addition of cetyltrimethylammonium bromide (CTAB) during core synthesis enhanced particle dispersion. Two silica coating conditions showed the greatest efficiency in the enhancement of ROS generation. Furthermore, our *in vivo* study revealed suppression of tumor growth by $Y_2O_3$:Eu@$SiO_2$ administration when compared to non-treated control. Silica shell provides flexibility to conjugate moieties that specifically target to cancers. This nano-photosensitizer demonstrates the significant promise for overcoming limitations of conventional PDT and combating various cancers in clinical applications.

**Keywords:** activated photodynamic therapy (PDT); X-ray activated PDT (XPDT); nanoparticle (NP); photosensitizer (PS); nano-PS; Europium doped Yttrium oxide nanoparticles ($Y_2O_3$:Eu); silica coated $Y_2O_3$:Eu ($Y_2O_3$:Eu@$SiO_2$); reactive oxygen species (ROS)

## 1. Introduction

Photodynamic therapy (PDT) is a cancer therapeutic modality based on the combination of three factors: photosensitizer (PS), light with a specific wavelength, and the presence of molecular oxygen to drive the production of highly cytotoxic reactive oxygen species (ROS) [1]. While conventional PDT shows promise in the effective treatment of cancers, it is hindered by the limited photon penetration and photon excitation in tissues, suppressed efficiency of PS due to multiple energy

 doi:10.20944/preprints202405.1623.v1



transfers, and insufficient oxygen source in hypoxic tumor microenvironments [2]. These limitations restrict PDT to only superficial tissues and those that can be readily accessed either endoscopically or laparoscopically, which are due to the intrinsic scattering and absorption of photons by intervening tissues [2].

X-ray induced photodynamic therapy (XPDT) is a nascent modality designed to impart precisely targeted, relatively low-dose radiation directly to the tumor microenvironment using europium-doped yttrium oxide ($Y_2O_3$:Eu) nanoparticle (NPs) as nano-PS for deep-tissue cancer therapy. In the case of $Y_2O_3$:Eu NPs, the excitation energy is first absorbed by the host lattice. The electrons of the NPs are then promoted across the band gap to the conduction band which creates holes in the valence band. The observed ROS generation is a result from electrons in the conduction band and holes in the valence band exhibiting high reducing and oxidizing power, respectively [2].

The use of $Y_2O_3$:Eu as a scintillator for medical imaging, radiation detection, and dosimetry has been extensively studied [3] and reviewed [4]. Indeed, $Y_2O_3$:Eu NPs have demonstrated to be promising materials for *in situ*, *in vivo* x-ray dosimetry [5]. In addition, studies have shown that silica-coated $Y_2O_3$:Eu ($Y_2O_3$:Eu@$SiO_2$) NPs act as independent nano-PS for XPDT by generating an increased amount of ROS under X-ray irradiation, leading to cancer cell death [2]. While individual studies have been conducted to study the efficacy of $Y_2O_3$:Eu@$SiO_2$ NP, the outcomes for cytotoxicity and tumor suppression have been varying [6–8]. We suspect that this variation is due to different levels of ROS generated by variations in $Y_2O_3$:Eu@$SiO_2$ NP production. However, the information on how these variations influence ROS generation is missing. Therefore, this study focuses on understanding the effects of different synthesis aspects on $Y_2O_3$:Eu@$SiO_2$ NP. The efficacy of ROS generation by the $Y_2O_3$:Eu@$SiO_2$ NP is also compared.

Furthermore, the tumor suppression effect of $Y_2O_3$:Eu@$SiO_2$ NPs was illustrated on a human ovarian tumor radiation sensitive CAOV3 mouse xenograft model, using radiation resistant SKOV3 mouse model as the negative control. The ovarian cancer model was chosen because ovarian cancer is the sixth most common cancer worldwide among women in developed countries and the most lethal of all gynecological malignancies. Despite aggressive surgery, chemotherapy, and radiotherapy the prognosis is poor, with a five-year survival rate of less than 30% [9]. The poor prognosis is evident by a recurrence rate in almost 25% of cases with early-stage disease and in more than 80% with more advanced stages [10–12] due to the resistance to the standard therapies. Through this study, we establish that $Y_2O_3$:Eu@$SiO_2$ NP could improve the radiotherapy efficacy by means of elevated ROS generation, thus demonstrating potential application of $Y_2O_3$:Eu@$SiO_2$ NP in XPDT to overcome radiation resistance in cancers.

We hypothesize that the strategy of XPDT combining $Y_2O_3$:Eu@$SiO_2$ NP as a nano-PS and low dose X-ray will provide a new modality in combating deep tissue cancers for a precise and efficient treatment outcome. To accomplish this, we have developed methods for synthesizing, modifying, and refining $Y_2O_3$:Eu@$SiO_2$ NP capable of generating extensive levels of ROS under X-ray activation.

## 2. Materials and Methods

### *2.1. Chemicals*

$Y(NO_3)_3$ (99.9%), urea (99%), dihydroethidium (DHE), dimethyl sulfoxide (DMSO, 99.7%), tetraethyl orthosilicate (TEOS, 98%), toluene (99.5%), hexane (98.5%), ethanol (EtOH, 100%), and phosphate buffer solution (PBS, pH 7.4) were purchased from Thermo Scientific (Waltham, MA, USA). $Eu(NO_3)_3$ (99.9%), cetyltrimethylammonium bromide (CTAB, 99%), ammonium hydroxide ($NH_4OH$), and (3-aminopropyl)triethoxysilane (APTES, 99%) were purchased from Sigma-Aldrich (St. Louis, MO, USA).

### *2.2. Syntheses of $Y_2O_3$:Eu Core Nanoparticles*

The protocols to synthesize $Y_2O_3$:Eu core NP are adapted from Chuang et al. [2]. Two variations of the core synthesis protocols are specified and detailed in Figure 1. For Protocol 1, chemicals were mixed in a 250 mL round-bottomed flask, stirred at ~775 rpm for five minutes at room temperature and then heated to 85˚C with continuous stirring for a specified condensation time. To understand the factors that affect the core size, $Y_2O_3$:Eu core NPs were first produced with the various urea

 doi:10.20944/preprints202405.1623.v1



concentrations (1.5, 2, 2.5, and 3 M) in the reaction with the condensation time at two hours. Then the condensation time was varied (1, 2, 3, 4 hours) with urea concentration at 2 M.

In Protocol 2, CTAB was introduced in the reaction mixture. The reaction mixture of $Y(NO_3)_3$, $Eu(NO_3)_3$, and CTAB was heated at 100˚C for one hour under vigorous stirring. Urea (4 M) was simultaneously heated at 40˚C for one hour. The two mixtures were then combined and heated at 100˚C for one hour while stirring vigorously.

At the end of the reactions, the white precipitate was collected through centrifugation (Sorvall ST8, Thermo Fisher, Waltham, MA, USA) and then washed with 15 mL double-distilled water ($ddH_2O$) three times, followed by one wash with 15 mL ethanol. The resulting $Y_2O_3$:Eu core NPs were dried overnight at 80˚C.

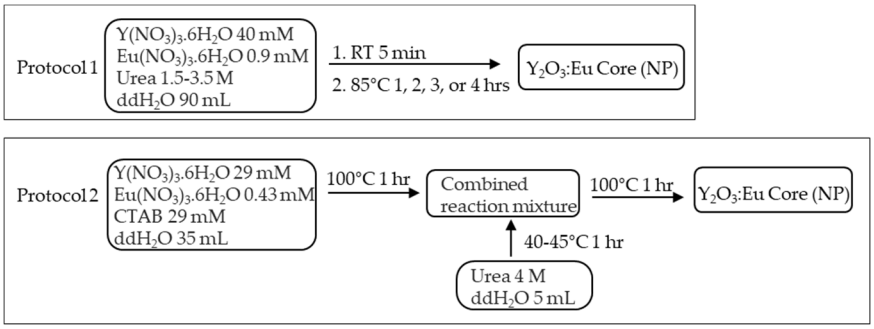


**Figure 1.** Protocols for $Y_2O_3$:Eu core nanoparticle syntheses.

*2.3. Silica Encapsulation of $Y_2O_3$:Eu Core Nanoparticles*

Five variations of the protocols were tested for the silica encapsulation of the $Y_2O_3$:Eu core NPs as depicted in Figure 2. The $Y_2O_3$:Eu core NPs produced without CTAB in the reaction were encapsulated with the Variation 5 condition only, while the $Y_2O_3$:Eu core NPs produced with CTAB were encapsulated with all 5 variations. At the end of reaction, the encapsulated $Y_2O_3$:Eu@$SiO_2$ NPs were collected through centrifugation and washed three times with 15 mL of a 1:1 solution of ethanol and $ddH_2O$. The obtained particles were then dried at 80˚C overnight.

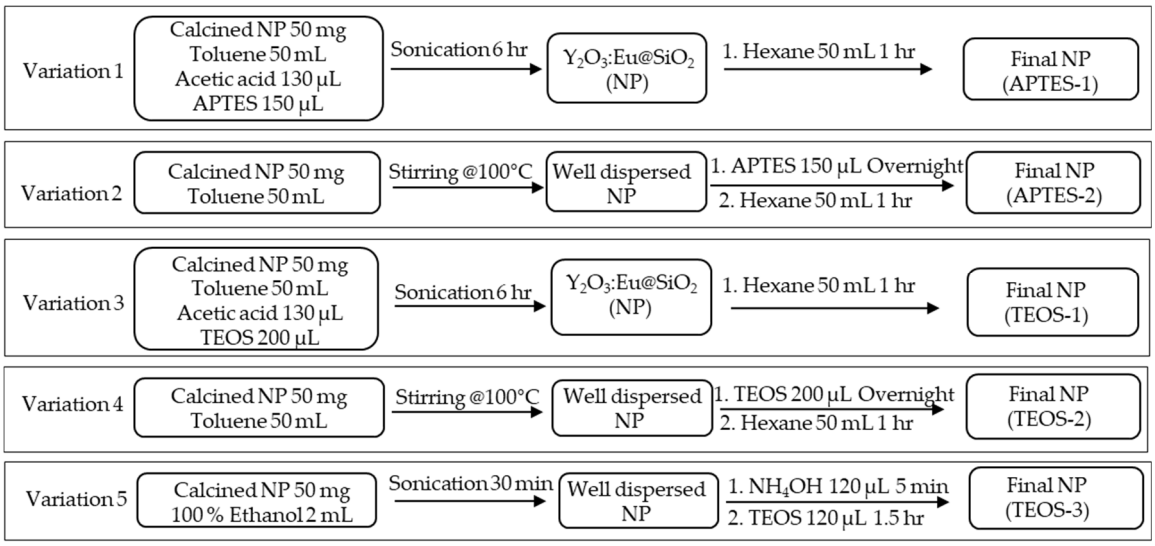


**Figure 2.** Protocols for silica encapsulation of $Y_2O_3$:Eu core nanoparticles.

*2.4. Calcination of the NP*

Dried NPs were calcinated at 800˚C for three hours. Calcination was performed either before and/or after the silica encapsulation. For the protocol when CTAB was present in the reaction, the calcination was done at 600˚C for 4 hours before the silica encapsulation. The final $Y_2O_3$:Eu@$SiO_2$ NPs were stored at 4˚C for further studies.

 doi:10.20944/preprints202405.1623.v1



*2.5. Transmission Electron Microscopy Measurement*

Particle morphology of $Y_2O_3$:Eu@$SiO_2$ NPs was characterized under transmission electron microscopy (TEM) (FEI, Hillsboro, Oregon, USA) at the Advanced Electron Microscopy Facility of the University of Chicago. $Y_2O_3$:Eu@$SiO_2$ NPs were first suspended in 100% ethanol (20 mg/mL), sonicated for 15 minutes, diluted 10 times in 100% ethanol, and sonicated for another 15 minutes. A final additional dilution of 10 times with 100% ethanol and sonication for 30 minutes was done before the $Y_2O_3$:Eu@$SiO_2$ NPs were imaged. The $Y_2O_3$:Eu core diameters and $SiO_2$ coating thicknesses were determined using the FIJI imaging analysis software. On average 109±30 (mean ± SEM) samples of NPs were measured for each batch of $Y_2O_3$:Eu@$SiO_2$ NPs.

*2.6. Measurement of ROS*

ROS measurements were done as described in Chuang et al.[2] with the following modifications. Briefly, $Y_2O_3$:Eu@$SiO_2$ NPs were suspended in phosphate buffered solution (PBS) (10 mg/mL) and sonicated for 15 minutes at 80 Hz and 100% power (FB11205 Ultrasonic Cleaner, Thermo Fisher, Waltham, MA, USA). To measure ROS production, the $Y_2O_3$:Eu@$SiO_2$ NP suspension (125 μg/mL) was mixed with DHE (10 μM) and irradiated at 1, 2, 4, and 8 Gy using a Phillips RT250 irradiator (Amsterdam, Netherland) followed by centrifugation for 5 minutes at 15,000 g. Supernatants (150 μL) were transferred to a black 96-well plate. The fluorescence was measured at a plate reader (Biotek, Winooski, VT, USA) with excitation/emission 480/576 nm. The results were expressed as the ratio ($I/I_0$) of the fluorescent intensity between the irradiated (I) and non-irradiated ($I_0$) samples. PBS without NPs was run parallel with $Y_2O_3$:Eu@$SiO_2$ NPs as negative control. The reaction mixtures were kept in the dark at all times.

*2.7. Cell Culture*

Human ovarian cancer radiation resistant SKOV3 and radiation sensitive CAOV3 cell lines were purchased from American Type Culture Collection (ATCC, Manassas, Virginia). SKOV3 and CAOV3 cells were cultured in McCoy's 5A (Thermo Fisher, Waltham, MA, USA) and DMEM (Thermo Fisher, Waltham, MA, USA) media supplemented with 10% fetal bovine serum respectively. All cells were incubated at 37°C in a humidified atmosphere of 5% $CO_2$.

*2.8. Tumor Xenograft*

All animal studies were performed in accordance with the guide for the care and use of laboratory animals from the Institutional Animal Care and Use Committee (IACUC) of National Health Research Institutes and approved by the IACUC at the University of Chicago. *In vivo* experiments were conducted using five to six-week-old Nu/Nu Athymic female mice (Envigo, Indianapolis, IN). Two million SKOV3 or CAOV3 cells were injected subcutaneously in the right hind leg. Tumors were monitored twice a week by caliper measurement and allowed to reach 250-400 $mm^3$ in volume before the treatment of $Y_2O_3$:Eu@$SiO_2$ NPs.

*2.9. Treatments of $Y_2O_3$:Eu@$SiO_2$ NP and Radiation*

The $Y_2O_3$:Eu@$SiO_2$ NPs were first conjugated with trimethyl-ammonia (TA) to improve solubility of the NPs before inoculation into the tumors as outlined in Figure 3A. The mice with CAOV3 tumors (n=5/group) were assigned to sham (CAOV3), and treatment (CAOV3-$Y_2O_3$:Eu@$SiO_2$) groups randomly. The treatment group received intra-tumoral injection of $Y_2O_3$:Eu@$SiO_2$-TA NPs (16 mg/kg BW) one hour prior to radiation therapy while the sham treated tumors received same volume of saline injection. A group of animals (n=5) with SKOV3 tumors served as negative controls. Image guided tumor irradiation was performed on all mice on an XRAD225Cx (Precision X-ray, North Branford, CT). Mice were irradiated with 2 Gy/day for 4 consecutive days.

*2.10 $^{18}$F-FLT PET Imaging*

 doi:10.20944/preprints202405.1623.v1



To determine tumor therapeutic response, $^{18}$F-fluorothymidine positron emission tomography ($^{18}$F-FLT PET) imaging was conducted at baseline and 1-, 4-, 7-, and 14-days post NP and radiation treatment (Figure 3B). Mice received ~150 μCi (5.55 MBq) of $^{18}$F-FLT (Cyclotron Facility, University of Chicago, Chicago, IL, USA) in 100 μL isotonic saline solution by tail vein injection. For each time point, CT images were acquired on the X-Cube preclinical microCT imaging system, (Molecubes, Gent, Belgium). CT images were reconstructed with a 200 μm isotropic voxel size and used for PET attenuation correction and anatomical reference. One hour after $^{18}$F-FLT injection, 20 minutes static PET scans were acquired on the β-Cube preclinical microPET imaging system (Molecubes, Gent, Belgium) with 133 mm × 72 mm field of view (FOV) and an average spatial resolution of 1.1 mm at the center of FOV. List-mode data were reconstructed using a three-dimensional OSEM algorithm with a 400 μm isotropic voxel size. Animals were maintained under ~2% isoflurane anesthesia in oxygen during imaging procedures. Respiratory rate and body temperature were constantly monitored and maintained using Molecubes on-board physiological monitoring interface.

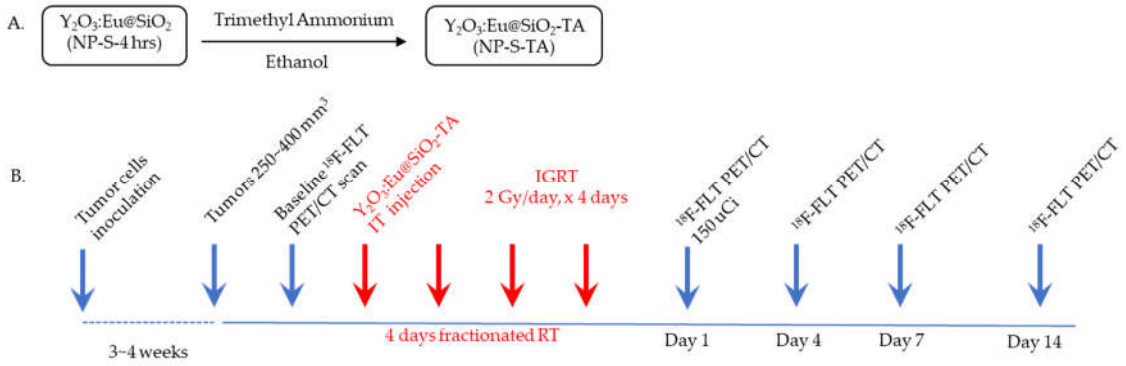


**Figure 3.** *In vivo* study protocol. A. $Y_2O_3$:Eu@$SiO_2$ NP functionalization protocol. B. $Y_2O_3$:Eu@$SiO_2$ NP treatment of tumor xenograft of human ovarian cancer and $^{18}$F-FLT PET imaging. .

*2.11. Image Analysis*

All image analysis was performed with VivoQuant software (Invicro, LLC, Boston, MA, USA). 3D regions of interest (ROIs) were drawn and standardized uptake values (SUVs) and percent injected dose per gram of tissue (%ID/g) were calculated for each ROI and time point. SUV is defined as:

$$SUV = \frac{radioactivity\ concentration\ in\ volume\ of\ interest\ (VOI)(\frac{\mu Ci}{mL})}{\frac{\text{injected dose (}\mu\text{Ci)}}{\text{body weight of animal (g)}}}$$

%ID/g was calculated as a ratio of tissue radioactivity concentration (mCi/g) at time of scan to total injected activity (mCi) at time of scan.

*2.12 Statistics*

Statistical analyses were performed using Prism software (GraphPad, La Jolla, CA, USA). Average data were presented as means ± SD or means ± SEM as specified in the results. Differences between groups were determined by one-way or two-way ANOVA using the Bonferroni post hoc test. The correlation analyses were done using simple linear regression. $P < 0.05$ was considered statistically significant.

**3. Results**

To understand the impact of synthesis conditions on $Y_2O_3$:Eu@$SiO_2$ NP morphology, TEM imaging was performed after the NP production. $Y_2O_3$:Eu@$SiO_2$ NP core diameters and silica coat thickness were measured using FIJI image analysis software on the TEM images. Similarly, the impact that synthesis conditions have on ROS generation were quantified using DHE fluorescent probe.

 doi:10.20944/preprints202405.1623.v1



Finally, the efficacy of X-ray activated $Y_2O_3$:Eu@$SiO_2$ NPs were evaluated *in vivo* using human ovarian tumor xenograft tumor model in mice. Results are presented in the following sections.

### *3.1 Effects of Synthesis Condition on Size of $Y_2O_3$:Eu@$SiO_2$ Core*

As shown in Figure 4A, under the fixed urea concentration of 2 M, a significant direct correlation ($R^2 = 0.7357$, $p < 0.05$) was observed between condensation time of the $Y_2O_3$:Eu@$SiO_2$ NP synthesis reaction and the diameter of the resulting NP cores. On average, 98±3 (mean ± SEM) samples of $Y_2O_3$:Eu@$SiO_2$ NP cores were measured. NP cores increased in size from 36±6 nm (mean ± SD) for 1 hour of condensation to 205±24 nm (mean ± SD) for four hours of condensation. In contrast, Figure 4B shows a significant negative correlation ($R^2 = 0.958$, $p < 0.05$) between urea concentration in the synthesis solution and the resulting NP core diameter with condensation time of four hours. Core diameter decreased substantially in size from 176±13 nm (means ± SD) for 1.5 M urea to 75±6 nm (means ± SD) for 3.5 M urea.

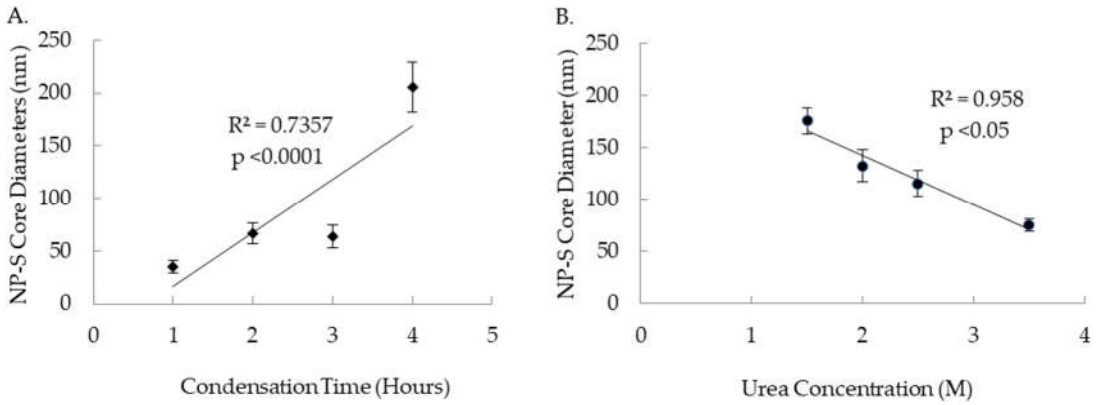


**Figure 4.** Effects of condansation time and urea concentration on core size. A. Plot of $Y_2O_3$:Eu@$SiO_2$ NP core diameter (nm) versus condensation time (hours) shows that core diameter increases with longer condensation period ($R^2 = 0.7357$, $p < 0.05$). B. Plot of $Y_2O_3$:Eu@$SiO_2$ NP core diameter (nm) versus urea concentration (M) shows an inverse relationship between the urea concentration and core diameter ($R^2 = 0.958$, $p < 0.05$).

### *3.2. Effects of Silica Coating Conditions and Calcination on Thickness of $Y_2O_3$:Eu@$SiO_2$ Shell*

As shown in Figure 5, examination of the silica coating thickness revealed notable differences between $Y_2O_3$:Eu@$SiO_2$ NP encapsulation conditions with different solvents during silica deposition. NP made using toluene and hexanes as the solvent consistently had silica coats of approximately 4 nm thickness. In comparison, particles made using ethanol as the solvent without hexanes demonstrated thicker silica shell of 9±1 nm (mean ± SEM). In addition, Figure 5 demonstrates the timing of calcination influenced the silica deposition on to the surface of the $Y_2O_3$:Eu core. Both calcination before (CB) the encapsulation alone and calcination before and after (CBCA) the encapsulation produced thicker silica shell than calcination after (CA) encapsulation. No differences in coat thickness were observed between the calcination Timing of CB and CBCA.

### *3.3. Effects of Synthesis Conditions on the Dispersibility of $Y_2O_3$:Eu@$SiO_2$ NP*

A representative TEM image from each synthesis condition is displayed in Figure 6. The cores of $Y_2O_3$:Eu@$SiO_2$ NP in CB, CA and CBCA groups were synthesized without CTAB, while the other groups included CTAB in the reaction mixture. In these images, the $Y_2O_3$:Eu@$SiO_2$ NP in CB, CA and CBCA group (without CTAB) appear to be clustered while $Y_2O_3$:Eu@$SiO_2$ NP in the other groups (with CTAB) appear evenly distributed, suggesting that the presence of CTAB in the NP core sythesis improves the dispersity of the NP.

Preprints.org (www.preprints.org) | NOT PEER-REVIEWED | Posted: 24 May 2024 doi:10.20944/preprints202405.1623.v1



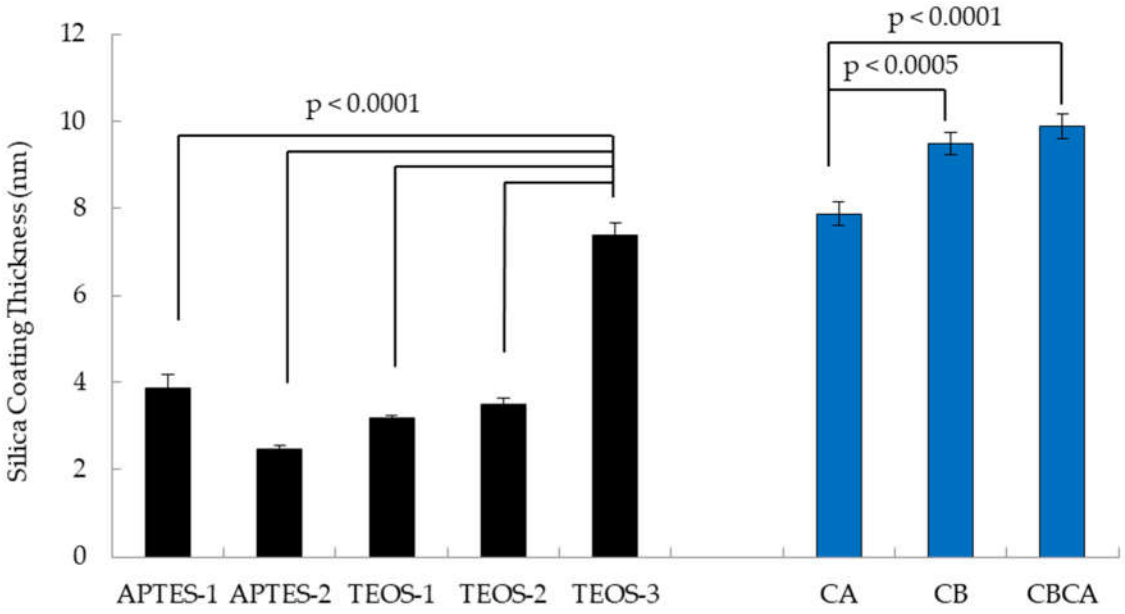


**Figure 5.** Effects of various silica coating techniques and calcination placements on thickness of silica coat on $Y_2O_3$:Eu@$SiO_2$ NP. Silica coating conditions for APTES-1, APTES-2, TEOS-1, and TEOS-2 yeilded similar thickness while the condition for TEOS-3 produced a thicker coating than the others ($p < 0.0001$). Calcination condition of CA yielded thinner silica coats than CB and CBCA ($p < 0.0001$ & $< 0.0005$). (CA: Calcination after silica coating; CB: Calcination before silica coating; CBCA: Calcination before and after silica coating).

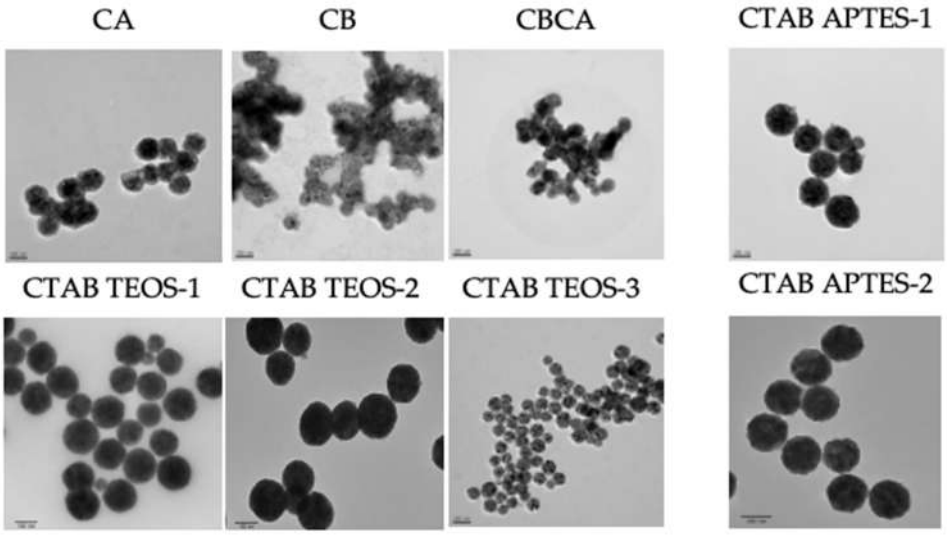


**Figure 6.** Representative TEM images of $Y_2O_3$:Eu@$SiO_2$ NP produced under various conditions shows that the addition of CTAB during core synthesis produced NP with better dispersity. (TEM magnifications: CA, CB, CBCA, CTAB TEOS-3, CTAB APTES-1: 39,000x; CTAB TEOS-1: 40,000x; CTAB TEOS-2, CTAB APTES-2: 50,000x).

### *3.4. Effects of Synthesis Condition on the ROS Generation*

Quantitation of ROS generation by DHE fluorescent probe showed that all $Y_2O_3$:Eu@$SiO_2$ NPs generated progressively higher ROS with increasing radiation dose from 0 to 8 Gy (Figure 7). However, the extent of ROS production varied between NPs. Figure 7A shows the ROS generation by different silica coating protocols on the $Y_2O_3$:Eu@$SiO_2$ NP produced with CTAB addition. Under

 doi:10.20944/preprints202405.1623.v1



similar coating conditions, using APTES as silica source enhanced x-ray induced ROS generation (APTES-1 vs TEOS-1 and APTES-2 vs TEOS-2). Higher ROS generation was also observed from NPs with addition of the silica sources at the beginning of the reaction (APTES-1 vs APTES2 and TEOS-1 vs TEOS-2). Overall, TEOS-3 and APTES-1 have the highest ratio of fluorescence intensity, indicating significant ROS generation. TEOS-1 and APTES-2 showed modestly elevated ROS over the PBS control that was not statistically significant, and TEOS-2's ROS generation is similar to that of PBS (Figure 7A.) ROS generation for $Y_2O_3$:Eu@$SiO_2$ NPs synthesized with different calcination protocols is shown in Figure 7B. CA showed a small increase in ROS compared to PBS control at 8 Gy but not at other radiation doses with no statiscal difference overall. The ROS generation of CB and CBCA is similar to that of PBS. Figure 7C highlights the significantly greater ROS production of TEOS-3 and APTES-1 than $Y_2O_3$:Eu@$SiO_2$ NP produced with other formulations or coating protocols at both 4 Gy and 8 Gy radiation doses. No correlation was found between the ROS production and the size of $Y_2O_3$:Eu@$SiO_2$ NP core, nor the silica coat thickness (data not shown).

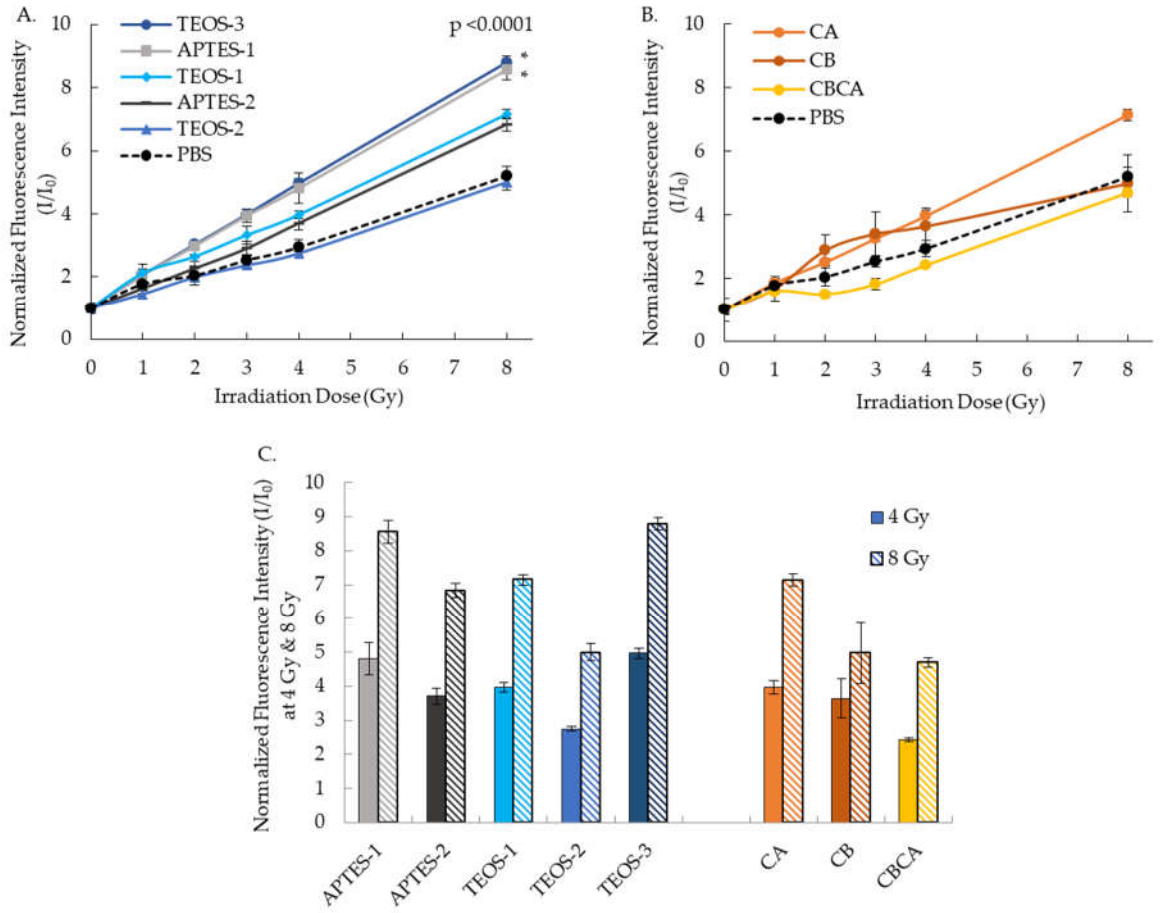


**Figure 7.** Effect of NP synthesis on x-ray induced ROS production measured by DHE fluorescent probe. A. Effects of silica coating on the normalized fluorescent intensity under 0-8 Gy irradiation. B. Effects of calcination on the normalized fluorescent intensity under 0-8 Gy irradiation. C. Normalized fluorescent intensity prodeced at 4 & 8 Gy irradiation demonstrates significance of TEOS-3 and APTES-1.

### *3.5. In vivo Evaluation of the $Y_2O_3$:Eu@$SiO_2$ NP in a Human Ovarian Cancer Xenograft Model*

To evaluate the efficacy of $Y_2O_3$:Eu@$SiO_2$ NP XPDT, tumor cell proliferation was evaluated before treatment and up to 14 days after treatment by PET imaging using $^{18}$F-FLT. Figure 8A shows representative axial sections of SUV scaled PET images at each time point for the three animal groups. $^{18}$F-FLT uptake decreased for both sham and $Y_2O_3$:Eu@$SiO_2$ NP CAOV3 tumors from Day 1 post treatment and remained suppressed. Radiation resistant SKOV3 xenografts showed a similar but

 doi:10.20944/preprints202405.1623.v1



temporary response at Day 1 and overall uptake was not significantly different across the 14 days (Figure 8B). However, when comparing both radiation sensitive CAOV3 groups to the SKOV3, the decrease in uptake at Day 4, 7, and 14 was significantly different, measuring about 55% for the CAOV3 xenografts treated with NP, about 40% for the sham CAOV3, and 19%, 3% and 13% at Day 4, 7, and 14 respectively for SKOV3 (Figure 8C). Tumor volume was monitored by caliper measurement, and changes in volume relative to baseline show significant growth in SKOV3 xenograft, with over 400% increase over 14 days, while CAOV3 tumors grew at a slower rate, reaching about 40% increase at Day 4, before reducing in size, measuring about 45% lower volume at Day 14 (Figure 8D).

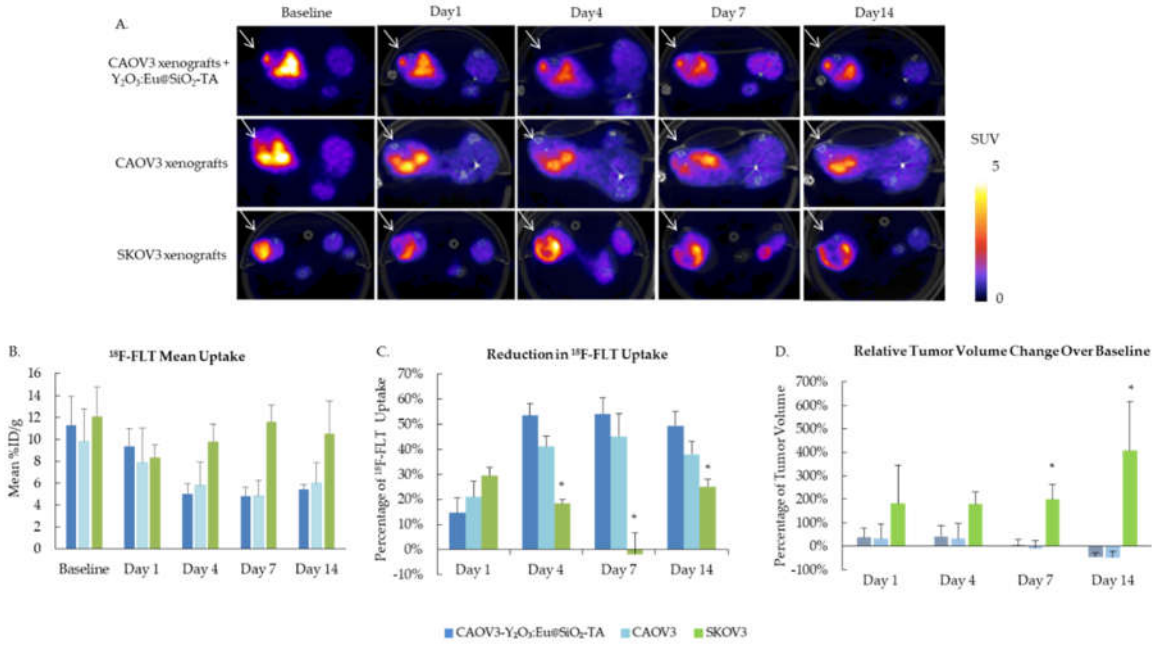


**Figure 8.** Intra-tumor $Y_2O_3$:Eu@$SiO_2$ treatment enhanced the radiation induced growth suppression of radiation sensitive CAOV3 xenografts. A. Representative images of $^{18}$F-FLT PET imaging demonstrate the lowered tumor proliferation in NP treated tumor xenograft. B. Mean $^{18}$F-FLT uptake and C. Reduction in $^{18}$F-FLT uptake reveals enhanced tumor suppression effects of $Y_2O_3$:Eu@$SiO_2$ NP (*$p < 0.05$). D. Reduction of relative tumor volume in CAOV3 xenograft measured by caliper. (n=3, mean ± SD).

## 4. Discussion

### *4.1. Assessment of Synthesis Protocols and the Relevant Conditions and Factors Affecting the Characteristics of $Y_2O_3$:Eu@$SiO_2$ NPs*

Typically, $Y_2O_3$:Eu@$SiO_2$ NP core production uses an urea-assisted precipitation procedure [4]. $Y_2O_3$:Eu@$SiO_2$ NPs produced using this procedure has previously shown effectiveness in the generation of ROS, increased cytotoxicity, and enhanced tumor suppression in ovarian cancer xenografts [2]. We evaluated the factors in this procedure that may influence the outcome of $Y_2O_3$:Eu@$SiO_2$ NP. It is found that urea concentration is strongly and inversely correlated with the final size of the NP core, while a positive correlation with the longer reaction condensation time leading to a larger final NP core size was also demonstrated in our study (Figure 1).

The size of the $Y_2O_3$:Eu@$SiO_2$ NP plays key roles in influencing their *in vivo* transport, pharmacokinetics, and cellular interaction [13]. In addition, the NP size is critical to successful delivery to tumors. Research has shown that the size of NP should be tailored depending on the type and the location of the tumor [14]. In this aspect, our study will serve as a basic guidance on how the $Y_2O_3$:Eu@$SiO_2$ NP size can be manipulated by the synthesis procedure. To the best of our knowledge, no such data is currently available.

 doi:10.20944/preprints202405.1623.v1



More importantly, we also tested a synthesis condition in which CTAB was incorporated for the $Y_2O_3$:Eu@$SiO_2$ NP production. From the TEM images, the addition of CTAB seemed to result in NP with better dispersity. The NP size was not affected by the presence of CTAB in the reaction mixture (average core diameter of 69 nm vs 68 nm, data not shown). Dynamic light scattering (DLS) methods, which will be conducted in future studies, will provide more quantitative assessment of the $Y_2O_3$:Eu@$SiO_2$ NP size distribution.

In addition to characterizing the synthesis conditions of $Y_2O_3$:Eu@$SiO_2$ NP core formation, we also compared the effects of five different silica coating protocols for the thickness of encapsulation. The coating condition with ethanol solvent yielded thicker silica coats than four other conditions using toluene and hexane as solvents. This observation implies that solvent polarity impacts the deposition of the silica coating with solvents like toluene and hexanes appearing to restrict silica deposition compared to polar solvents like ethanol. Interestingly, using either TEOS or APTES as a silica source did not affect the thickness of the silica coating.

Our results also suggested the importance of the calcination timing in affecting silica deposition. Calcination prior to silica coating facilitated silica deposition. The second calcination after silica encapsulation in CBCA condition has no effect on the coating thickness. Calcination after silica coating presented with thinner silica shell.

Silica is believed to be one of the ideal coatings to preserve the quantum property of nanoparticles [15]. However, conflicting results have been reported. In 2007, [16] showed that a silica coating increased $Y_2O_3$:Eu luminescent intensity by potentially decreasing the surface defects of NP. In contrast, [17] reported the luminescent efficiency decreased with the increase of the thickness of the silica coating in 2019. We found no correlation between the X-ray induced ROS generation and thickness of the silica coating, or the size of the $Y_2O_3$:Eu@$SiO_2$ NP core. Instead, under similar reaction condition, NP coated using APTES as silica source have enhanced the ROS generation then using TEOS as a silica source, especially when it is added at the beginning of the silica deposition reaction.

Although this study did not show any significant effects of silica shell thickness on X-ray induced ROS generation, the coating thickness may affect the ligation of functional groups such as antibodies specific targeted to tumor surface protein. Conjugation of functional group is important for the *in vivo* application of $Y_2O_3$:Eu@$SiO_2$ NP. Further studies to understand the relationship of silica coating and functional group conjugation are warranted.

Overall, our study concluded that $Y_2O_3$:Eu@$SiO_2$ NP synthesized with CTAB addition (Figure 1, Protocol 2) and silica coating using either APTES, toluene and hexane, or TEOS and $NH_4OH$ (Figure 2, Variation 1 and 5) generated most ROS. Future studies will include the *in vivo* efficacy of tumor therapy using these NPs synthesized through the select protocols indicated above to investigate and ultimately establish quantitative correlation between therapeutic outcomes and ROS generation levels, and in turn, the optimal choice of $Y_2O_3$:Eu@$SiO_2$ NP synthesis protocol and the related parametric options that could be tailored to the specific therapeutic requirements dictated by the individual "patient" subject conditions, paving ways leading to translation to future practice of "personalized" therapy and medicine.

### *4.2. In Vivo Evaluation of the $Y_2O_3$:Eu@$SiO_2$ NP in a Human Ovarian Cancer Xenograft Model*

The illustrative *in vivo* evaluation conducted in an ovarian cancer mouse xenograft model demonstrated promising tumor suppression capabilities of the $Y_2O_3$:Eu@$SiO_2$ NPs (Figure 8). These preliminary results suggest the potential of the engineered $Y_2O_3$:Eu@$SiO_2$ NPs to suppress radiation-resistant tumor progression *in vivo*, through ROS production.

It is important to note that this preliminary evaluation study was carried out before the systematic investigation of NPs synthesis protocols and related experimental parameters and factors, of which the study results were reported earlier in this paper. Therefore, the synthesis approach and experimental conditions employed to produce the $Y_2O_3$:Eu@$SiO_2$ NPs used in the *in vivo* study were the ones utilized during the early phase of this ongoing project, which was by no means optimized. Hence, the therapeutic effects demonstrated in this preliminary study were also not optimized. As discussed already in Section 4.1, systematic investigation of optimization of synthesis protocols and relevant experimental parameters and factors, and their relationship of the therapeutic outcomes, will be carried out in the future, which will definitely include *in vivo* experiments employing animal

 doi:10.20944/preprints202405.1623.v1



models as part of the evaluation in the real-world preclinical environment, and ultimately translation to clinical human trials.

## 5. Conclusion

Our studies and their results reported here provided important information on the syntheses of $Y_2O_3$:Eu@$SiO_2$ NP. This nano-photosensitizer has also been demonstrated in preliminary *in vivo* evaluation to offer significant promise for overcoming limitations of conventional PDT and potentially capable of combating various cancers in a wide range of clinical applications. Our research team continues to carry out systematic investigation toward establishing quantitative correlation between NPs synthesis methods utilized and therapeutic outcomes via XPDT practice, with the ultimate goal of moving toward practice of personalized medicine in the future.

**Author Contributions:** Conceptualization, L.-W.L.; C.-T.C.; methodology, H.J.Z.; M.S.; L.L.; J.S.S.; S.-H.C.; N.-T.C.; L.-W.L.; C.-T.C.; investigation, H.J.Z.; T.I.; M.S.; L.L.; J.S.S.; S.-H.C.; N.-T.C.; L.-W.L.; C.-T.C.; data curation, H.J.Z.; T.I.; M.S.; L.L.; E.T.; A.P..; formal analysis, H.J.Z.; T.I.; L.L.; D.B.; E.T.; A.P.; writing—original draft preparation, H.J.Z.; T.I.; L.L.; D.B.; writing—review and editing, M.S.; J.S.S.; E.T.; A.P.; S.-H.C.; N.-T.C.; L.-W.L.; C.-T.C.; resources, H.J.Z., M.S., L.L.; L.-W.L.; C.-T.C.; supervision, L.-W.L.; C-T.C.; project administration, H.J.Z.; L.L.; L.-W.L.;C.-T.C.; funding acquisition, J.S.S.; L.-W.L.; C.-T.C. All authors have read and agreed to the published version of the manuscript.

**Funding:** This research was funded in part by the University of Chicago (UChicago) Department of Radiology Pilot Seed Grant; by the UChicago Comprehensive Cancer Center (UCCCC) Program-Specific Pilot Grant through the NIH Cancer Center Support Grant P30 CA014599; by the NIH Shared Instrumentation Grant S10 OD025265 to the UChicago Integrated Small Animal Imaging Research Resource (iSAIRR); by the National Science and Technology Council, Taiwan, Grant 12D2-BNNSTC04; and by the National Health Research Institutes, Taiwan, Grant 13A1-BNPP04-014.

**Institutional Review Board Statement:** The animal study protocol was approved by the Institutional Animal Care and Use Committee of The University of Chicago (ACUP-72231).

**Data Availability Statement:** The data presented in this study are available on request from the corresponding authors. The data are not publicly accessible because they are not available in a format that is sufficiently accessible or reusable by other researchers.

**Acknowledgments:** We are grateful for the support from The Cyclotron Facility and the iSAIRR of the University of Chicago. We are also thankful for the contribution by Dr. Hye-Yeong Kim to the project.

**Conflicts of Interest:** The authors declare no conflict of interest. The funders had no role in the design of the study; in the collection, analyses, or interpretation of data; in the writing of the manuscript; or in the decision to publish the results. Certain commercial equipment, instruments, or materials are identified in this paper to foster understanding. Such identification does not imply recommendation by the authors or their affiliated institutions, nor does it imply that the materials or equipment identified are necessarily the best available for the purpose.

**Sample Availability:** Not available.

## References

1. Lee, C.-N.; Hsu, R.; Chen, H.; Wong, T.-W. Daylight photodynamic therapy: an update. *Molecules* **2020**, *25*, 5195.
2. Chuang, Y.-C.; Chu, C.-H.; Cheng, S.-H.; Liao, L.-D.; Chu, T.-S.; Chen, N.-T.; Paldino, A.; Hsia, Y.; Chen, C.-T.; Lo, L.-W. Annealing-modulated nanoscintillators for nonconventional x-ray activation of comprehensive photodynamic effects in deep cancer theranostics. *Theranostics* **2020**, *10*, 6758–6773.
3. Cavouras, D.; Kandarakis, I.; Panayiotakis, G.S.; Evangelou, E.K.; Nomicos, C.D. An evaluation of the $Y_2O_3$:$Eu^{3+}$ scintillator for application in medical x-ray detectors and image receptors. *Medical Physics* **1996**, *23*, 1965–1975.
4. 4. Souris, J.S.; Leoni, L.; Zhang, H.J.; Pan, A.; Tanios, E,; Tsai, H.-M.; Balyasnikova, I.V.; Bissonnette, M.; and Chen, C.-T.: X-ray activated nanoplatforms for deep tissue photodynamic therapy. *Nanomaterials* **2023**, 13(4):673.
5. Souris, J.S.; Cheng, S.-H.; Pelizzari, C.; Chen, N.-T.; La Riviere, P.; Chen, C.-T.; Lo, L.-W. Radioluminescence characterization of in situ x-ray nanodosimeters: potential real-time monitors and modulators of external beam radiation therapy. *Appl Phys Lett* **2014**, *105*, 203110.

 doi:10.20944/preprints202405.1623.v1




6. Cannas, C.; Casu, M.; Mainas, M.; Musinu, A.; Piccaluga, G. Synthesis and characterization of $Y_2O_3/SiO_2$ composites. *Zeitschrift für Naturforschung A* **2004**, *59*, 281–287.
7. Goswami, B.; Rani, N.; Ahlawat, R. Structural and optical investigations of $Nd^{3+}$ doped $Y_2O_3$-$SiO_2$ nanopowder. *Journal of Alloys and Compounds* **2018**, *730*, 450–457.
8. Porosnicu, I.; Butnaru, C.M.; Tiseanu, I.; Stancu, E.; Munteanu, C.V.A.; Bita, B.I.; Duliu, O.G.; Sima, F. $Y_2O_3$ nanoparticles and x-ray radiation-induced effects in melanoma cells. *Molecules* **2021**, *26*, 3403-3418.
9. Modugno, F.; Edwards, R.P. Ovarian cancer: prevention, detection, and treatment of the disease and its recurrence. Molecular Mechanisms and Personalized Medicine Meeting Report. *Int J Gynecol Cancer* **2012**, *22*, S45-57.
10. Salani, R.; Backes, F.J.; Fung, M.F.K.; Holschneider, C.H.; Parker, L.P.; Bristow, R.E.; Goff, B.A. Posttreatment surveillance and diagnosis of recurrence in women with gynecologic malignancies: society of gynecologic oncologists recommendations. *Am J Obstet Gynecol* **2011**, *204*, 466–478.
11. Armstrong, D.K.; Bundy, B.; Wenzel, L.; Huang, H.Q.; Baergen, R.; Lele, S.; Copeland, L.J.; Walker, J.L.; Burger, R.A. Intraperitoneal cisplatin and paclitaxel in ovarian cancer. *N Engl J Med* **2006**, *354*, 34–43.
12. Trimbos, J.B.; Parmar, M.; Vergote, I.; Guthrie, D.; Bolis, G.; Colombo, N.; Vermorken, J.B.; Torri, V.; Mangioni, C.; Pecorelli, S.; Lissoni, A.; Swart, A.-M. International collaborative ovarian neoplasm trial 1 and adjuvant chemotherapy in ovarian neoplasm trial: two parallel randomized phase III trials of adjuvant chemotherapy in patients with early-stage ovarian carcinoma. *J Natl Cancer Inst* **2003**, *95*, 105–112.
13. Xu, M.; Qi, Y.; Liu, G.; Song, Y.; Jiang, X.; Du, B. Size-dependent in vivo transport of nanoparticles: implications for delivery, targeting, and clearance. *ACS Nano* **2023**, *17*, 20825–20849.
14. Hoshyar, N.; Gray, S.; Han, H.; Bao, G. The effect of nanoparticle size on in vivo pharmacokinetics and cellular interaction. *Nanomedicine* **2016**, *11*, 673–692.
15. Mulvaney, P.; Liz-Marzán, L.M.; Giersig, M.; Ung, T. Silica encapsulation of quantum dots and metal clusters. *J. Mater. Chem.* **2000**, *10*, 1259–1270.
16. Liu, G.; Hong, G.; Dong, X.; Wang, J. Silica-coated $Y_2O_3$:Eu nanoparticles and their luminescence properties. *Journal of Luminescence* **2007**, *126*, 702–706.
17. Ansari, A.A.; Khan, A.; Labis, J.P.; Alam, M.; Aslam Manthrammel, M.; Ahamed, M.; Akhtar, M.J.; Aldalbahi, A.; Ghaithan, H. Mesoporous multi-silica layer-coated $Y_2O_3$:Eu core-shell nanoparticles: synthesis, luminescent properties and cytotoxicity evaluation. *Materials Science and Engineering: C* **2019**, *96*, 365–373.